WELDING RESEARCH

SUPPLEMENT TO THE WELDING JOURNAL, NOVEMBER 1974

Sponsored by the American Welding Society and the Welding Research Council

Understanding the Role of Inclusions and Microstructure in Ductile Fracture

Effects of welding process variations on toughness are best understood by studying the weldment microstructure and inclusion size distribution

BY D. C. HILL AND D. E. PASSOJA

ABSTRACT. Much attention has been devoted to predicting and controlling fracture toughness in ferrous weldments. Extensive studies relating toughness with welding parameters and weldment composition have been made. All such studies have sought to define the important variables affecting toughness. Unfortunately, such studies often resulted in linear regressions of one variable against toughness, fracture mode was not held constant, and no efforts were made to relate the variable investigated to quantitative features of the weldment microstructure.

This work studied the effect of shielding gas on the resultant weldment microstructure and inclusion distribution in the GMA process. Quantitative techniques were established for the investigation of these features. The results are discussed in terms of weldment deoxidation, nucleation and growth of inclusions, and the effect of alloy balance on microstructure.

It is concluded that the mechanical properties of weldments fabricated from E70S-3 electrodes by the GMA process are dependent on both microstructure and inclusion size distribution. Optimum strength and toughness resulted when Ar-2% O_2 or Ar-25% CO_2 shielding gas was used in preference to CO_2 shielding gas.

D. C. HILL is Group Leader, Linde Research Department and D. E. PASSOJA is Research Scientist, Central Scientific Laboratory, Union Carbide Corporation, Tarrytown, New York.

Introduction

General

Considerable attention has been devoted to predicting and to controlling the notch toughness of ferrous weldments. Extensive studies have been performed seeking to identify the primary variables affecting toughness within a given welding process-alloy system (Refs. 1-7). Depending upon the system, the variables studied may have been welding procedure (Refs. 1,2), shielding gas (Refs. 2,3), filler wire composition (Refs. 4-6), or microstructure (Ref. 7). In the final analysis, however, the significant variables affecting toughness are the weldment microstructure and chemical composition; welding parameters are important only insofar as they influence these variables. It is important to note that the major alloying elements, Mn, Si, Ni, etc., affect weldment material properties and microstructure; whereas, the impurity elements, P, S, O, primarily affect weldment toughness.

In studying ferrous fracture, many researchers have noted that the presence of P, S, O, and N has correlated with decreases in toughness (Refs. 1, 6, 8). Toughness losses per percent of impurity may be calculated from data in the literature. Some typical coefficients are listed in Table 1. It should be realized that the ranges of these coefficients are quite large. This is in marked contrast with similar coefficients developed for strength correlations (Ref. 9). The disadvantage of considering such correlations in this manner are:

1. Fracture modes are not considered and may not be constant.

Table 1 — Toughness Losses at Shelf Energy Per Percent of Impurity

Impurity	Toughness loss, ft-lb (kgf-m)	
S	1000-2000	(138.5-277)
P	2600-3300	(360-457)
O	650-1500	(90-208)
N	50-900	(69.3-125)

2. No physical insight is developed.

3. Lack of physical understanding of the problem makes generalizations difficult.

This paper will consider variations in toughness which occur under conditions of a constant fracture mode — ductile shear. In the ductile shear mode, the fracture surface is dimpled and inclusions are usually associated with dimples on a one to one basis (Ref. 10).

Fig. 1 — An inclusion acting as a microvoid nucleation site in a specimen plastically deformed in uniaxial tension at -51 C. Etchant, 2%nital; X750, reduced 38%

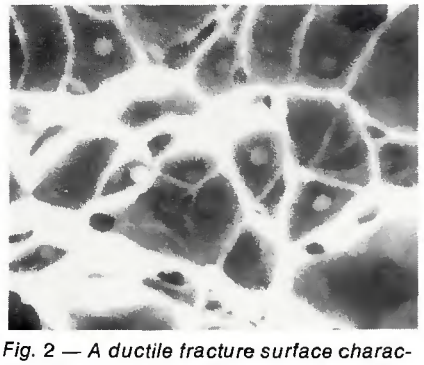

Fig. 2 — A ductile fracture surface characterized by dimples with associated inclusions. SEM X3500, reduced 38%

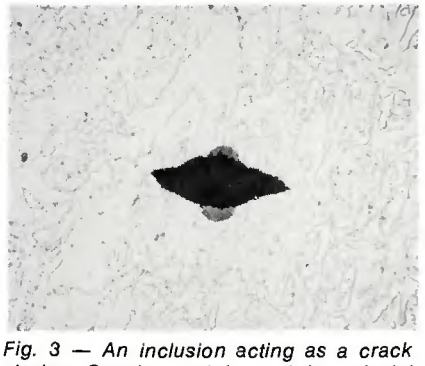

Fig. 3 — An inclusion acting as a crack starter. Specimen deformed in uniaxial tension at -51 C. Etchant, 2% nital; X400, reduced 38%

Inclusions and Fracture

Inclusions can participate in both ductile and brittle fracture. In ductile fracture they act as microvoid nucleation sites, Fig. 1. After nucleation, the voids grow, link up with microvoids growing in an adjacent region, and form a fracture surface. The general appearance of the fracture surface is shown in Fig. 2. In brittle fracture, inclusions can act as crack starters as illustrated in Fig. 3. This crack was formed by deforming under uniaxial tension at -51 C. Once nucleated the crack spread into the surrounding matrix as a brittle crack.

Inclusions and Notch Toughness

Two correlations between ductile fracture energy and inclusions have been shown to have broad applicability. Krafft (Ref. 11) introduced the tensile ligament instability concept and proposed that fracture toughness is related to a process zone size.

$$K = En\,(2\pi L)^{1/2} \qquad (1)$$

where K is the plane strain stress intensity factor, E is the elastic modulus, n is the work hardening coefficient and L is the process zone size. Spitzig (Ref. 12) and Birkle, et al (Ref. 13) demonstrated that this process zone size was apparently related to the spacing between sulfide particles. Passoja and Hill (Ref. 14) extended this approach and proposed that the process zone size can be related to the spacing between particles in the fracture plane involved in microvoid nucleation and growth. The essential conclusion of the tensile ligament instability concept is that fracture toughness is proportional to the mean inclusion spacing on a fracture surface. Another correlation is that of volume fraction of inclusions with notch toughness (Refs. 15-17). As the volume fraction increases, toughness decreases. Details of the inclusion size distribution or spatial separations have not been widely studied (Ref. 18).

Microstructure

Microstructural effects are known to influence toughness. There are generally two types of effects. The first is simply that related to the inherent fracture resistance of a transformation product; e.g., fine pearlite is generally tougher than coarse pearlite, tempered martensite is also usually tougher than lower bainite, fine ferrite is tougher than coarse ferrite, etc. The second is the influence of alloying elements on the mechanical properties of any transformation product; e.g., nickel is beneficial to ferritic structures.

It is important to realize that microstructural variations can be most important in understanding toughness variations, especially in mild or low alloy steels.

This Study

This study investigated the changes in microstructure and inclusion size distributions caused by shielding gas variations in the welding of E70S-3 electrodes with the GMA process. Techniques were developed to measure and to quantify salient features of the fracture surface. The influence of microstructure and inclusion distribution on mechanical properties was then demonstrated.

Experiments and Results

Weldment Preparation and Mechanical Testing

Weldments were fabricated using the automatic GMA process according to AWS Standard A5.18-69. The electrode satisfied AWS Class E70S-3. Baseplate was ¾ in. (1.89cm) A515 Grade. All welding was done in the flat position. Welding parameters are given in Table 2.

Standard full size Charpy V-Notch (CVN) specimens and 0.50 In. (1.26cm) tensile specimens were taken from the weldments in accordance with A5.18-69. The CVN specimens were tested at room temperature, −18 C and −51 C on a 240 ft-lb (33.2 kgf-m) Baldwin. Tensiles were pulled on a 10,000 lb (4536 kgf) Instron equipped with extensometer. Results of the mechanical tests are presented in Table 3.

Weldment Composition

Weldment composition was determined using quantitative emission spectroscopy for Mn, Si, and Cu. Carbon and sulfur were determined by combustion. Oxygen was measured using neutron activation. Weldment compositions are listed in Table 4.

Fracture Surface Investigations

The fracture surfaces of CVN impact specimens were investigated by means of a Cambridge Stereoscan Electron Microscope (SEM). By using a special adapter, the spec-

Table 2 — Welding Parameters

Weld	Shield gas	Current, A	Voltage, V	Heat input, kJ/in.(kJ/cm)
AR	Ar-2%O_2	210	23	32 (13)
A-C	Ar-25%CO_2	200	27	28 (11)
CO	CO_2	205	28	28 (11)

Table 3 — Mechanical Properties

Weld	YS, ksi (kgf/mm²)	UTS, ksi (kgf/mm²)	CVN, ft-lb (kgf-m) RT	−18 C	−51 C	Strain hard. coef.
AR	73 (51)	81 (57)	156(21.6)	106(14.7)	92(12.7)	0.148
A-C	70 (49)	77 (54)	125(17.3)	96(13.3)	70(9.7)	0.140
CO	58 (41)	65 (46)	79(10.9)	53(7.3)	7(1.0)	0.121

Table 4 — Weldment Compositions [a]

Weld	C	Mn	Si	Cu	O
AR	.08	1.00	.46	.18	.0416
A-C	.09	.78	.32	.18	.0438
CO	.08	.45	.12	.18	.0990

(a) Weight percent

imens were mounted so that the fracture surface was normal to the beam direction. Fracture surfaces were examined at magnifications from 800 to 2000 X. Fracture mode, density of inclusions, and mean linear intercept dimple size were measured. Data are given in Table 5.

The compositions of inclusions on the fracture surface were investigated using an EDAX x-ray analyzer. A general profile of the metallic content of the inclusions was developed and the inclusions were principally Mn and Si in the proper ratio for $MnSiO_3$. It was not possible to obtain an oxygen analysis by means of this technique.

Inclusion Studies

Carbon extraction replicas were made from the fracture surfaces. The replicas were used to determine the size distribution of inclusions on the fracture surface. It is important to note that the inclusions studied were active in the fracture process. Size counting was done by hand on electron micrographs taken from the replicas. Data are plotted as histograms in Fig. 4. The integrated data are shown on a probability plot in Fig. 5.

The inclusion density was calculated from these measurements. Data are presented in Table 6.

Inclusions collected on the extraction replicas were also analyzed using x-ray fluorescence and neutron activation. Their chemical composition was found to be approximately $MnSiO_3$.

Metallography

Transverse sections of each weldment were prepared using standard metallographic techniques. Etching was done with 2% nital. Representative photomicrographs are shown in Figs. 6 and 7.

Discussion

Comparative Weldment Mechanical Properties and Composition

Weldments AR and A-C had higher strengths than weldment CO. The strength difference for weldment AR is principally due to the solid solution strengthening of Mn; in comparison, for weldment A-C, increased strength results from solid solution strengthening of Mn and microstructural refinement due to higher carbon.

Weldments AR and A-C had superior impact properties. The primary differences between these weldments and weldment CO are that of lower oxygen content, thus a lower volume of inclusions, and higher Mn and Si content, thus different microstructures.

Depletion of alloying elements Mn and Si apparently lowers the work hardening coefficient in weldment CO.

The variation in the oxygen, Mn and Si contents of the weldments was caused by variations in the oxidation potential of the shield gas. For these experiments, CO_2 was significantly more oxidizing than Ar-2%O_2 or Ar-25%CO_2.

Inclusion Distributions

The inclusion size distributions measured on fractured surfaces revealed a larger mean inclusion diameter for weldment CO. Weldments AR and A-C had similar distributions, except at large inclusion diameters.

These distributions are consistent with what one would expect from classical nucleation and growth theory (Ref. 19). The liquid weld deposit contains Mn, Si, and oxygen. On cooling nuclei of the reaction product $MnSiO_3$ appear. As cooling continues the nuclei coarsen and more nuclei appear. The continuous processes of nucleation and growth continue until the melt is depleted of oxygen. At this point growth can continue by Ostwald ripening down to the solidification temperature and during thermal arrest during the solidification process. It follows that, since those melts containing the most oxygen will have the highest driving force for nucleation, they will nucleate at the highest temperatures and produce the distribution of inclusions with the largest mean diameters; e.g., weldment CO. For small increments of oxygen, only small variations are seen at the largest inclusion diameters; e.g., weldments AR and A-C.

By working on a fracture surface, only those inclusions participating in the fracture process were studied. Interestingly enough, the frequency

Table 5 — Fracture Mode, Mean Linear Intercept Dimple Size and Inclusion Density [a]

Weld	Fracture mode	Mean linear intercept dimple size, μm	Inclusion density, cm⁻²
AR	Ductile	1.53	1.61×10^7
A-C	Ductile	1.70	1.30×10^7
CO	Ductile	1.61	1.45×10^7

(a) All measured on specimens fractured at room temperature.

Table 6 — Inclusion Density and Areal Fraction from Extraction Replicas [a]

Weld	Inclusion density, cm⁻²	Areal fraction, % [b]
AR	1.31×10^7	1.61
A-C	1.60×10^7	2.19
CO	1.13×10^7	3.15

(a) Taken from specimens fractured at room temperature.
(b) In this case equal to 2.25 times the volume fraction.

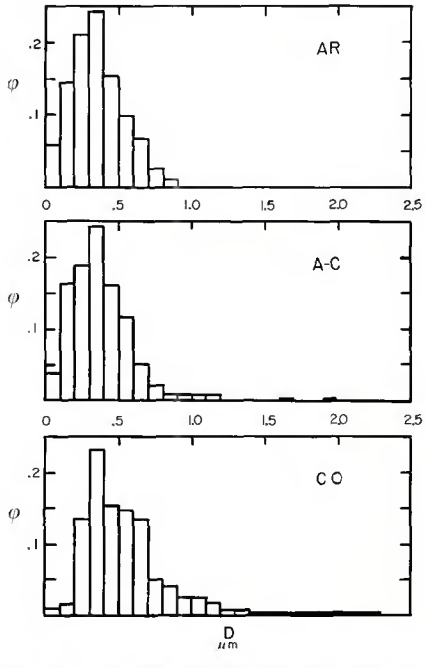

Fig. 4 — Frequency, ϕ, versus inclusion diameter, D, plotted for data taken from the fracture surfaces. Note that weldment AR has a much narrower range of diameters and smaller mean diameter than weldment CO

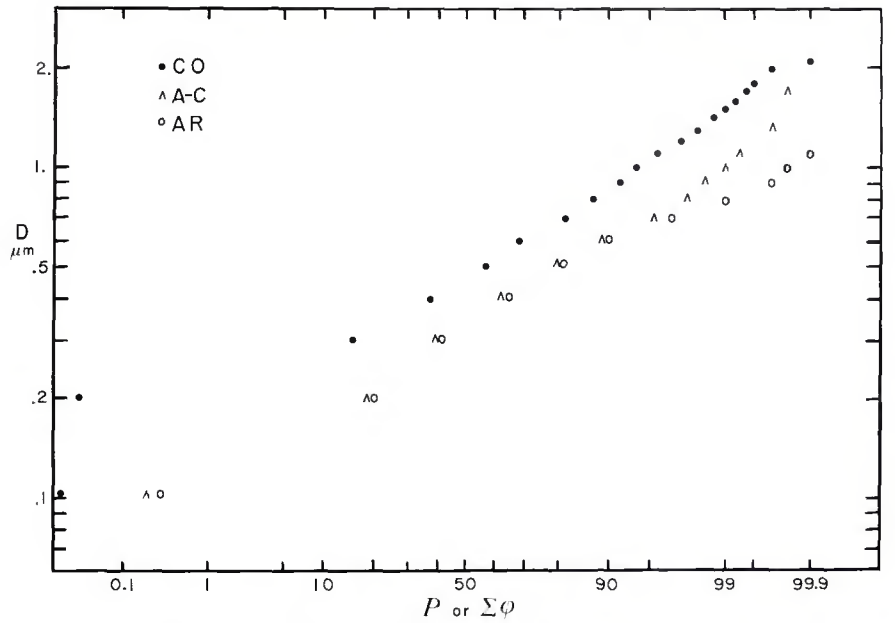

Fig. 5 — Diameter, D, plotted against the probability, P, or cumulative frequency, $\Sigma\phi$, for the data of Fig. 4. Note that weldment CO exhibits a larger mean diameter than weldments AR and A-C. Note also the minimum, or cut-off, diameter for weldment CO, at about 0.25 μ m. The plots suggest a cut-off diameter of about 0.15 μ m for weldments AR and A-C. Plots of this kind are inclusion size distributions

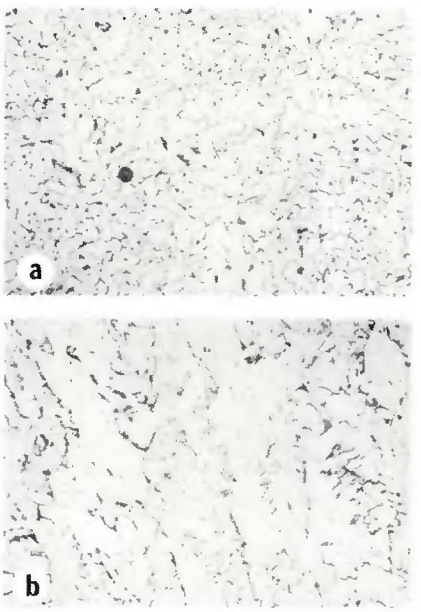

Fig. 6 — Photomicrographs of the refined (a) and unrefined (b) regions of weldment AR. Etchant, 2% nital; X400, reduced 38%

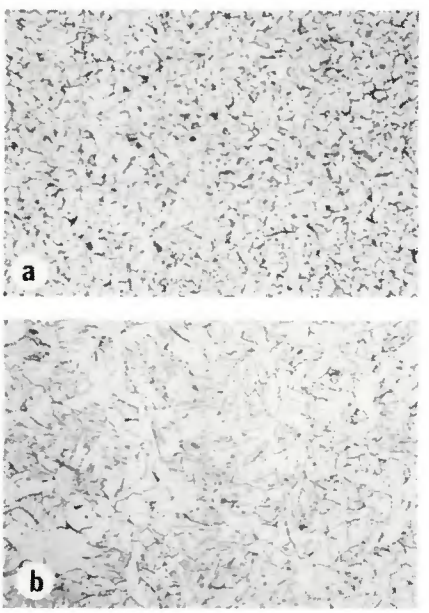

Fig. 7 — Photomicrographs of the refined (a) and unrefined (b) regions of weldment CO. Etchant, 2% nitəl; X400, reduced 38%

distributions measured in this work show the same log-normal distributions as measured by Widgery (Ref. 18) on cut and polished sections of weldments made in similar systems. An important difference is that this work indicates the existence of a minimum, or cut-off, inclusion size on the fracture surface. The implication is that only inclusions larger than the cut-off size are active in the fracture process.

The composition of the inclusions is $MnSiO_3$. This observation is entirely consistent with the thermodynamics of the deoxidation process active in the weldment.

The inclusion densities measured on the fracture surface are roughly equal for all the weldments. Because weldment CO has inclusions with a larger mean size, the volume fraction of inclusions is larger than for weldments AR and A-C. Since the inclusion densities are equal, the mean linear intercept dimple size is constant for these weldments. Thus there are an equal number of nuclei for microvoids, but the ductile fracture energies are different; hence the difference in energy must arise in the energy necessary to grow a microvoid. In the tensile ligament instability theory of Krafft (Ref. 11), this would be explained by increased strain hardening coefficient (see Eq. 1). Note that weldments AR and A-C have a higher work hardening coefficient than weldment CO. The qualitative trend of these results generally agrees with this hypothesis.

Microstructure Effects

The significant difference between the microstructures of weldments AR and CO was the ferrite substructure size. In comparing the same areas in both weldments, the substructure of weldment AR was finer than that of CO.

Summary and Conclusions

The mechanical properties of weldments fabricated from E70S-3 electrodes by the GMA process are dependent on shielding gas. Optimum strength and toughness results when Ar-2%O_2 or Ar-25%CO_2 shielding gas is used in preference to CO_2 shielding gas. As the oxidizing potential of the shielding gas is increased, more oxygen is dissolved in the weld puddle, thus consuming more Mn and Si. Inclusions nucleated at higher temperatures grow larger during cooling from the maximum super-heat temperature and during the solidification process. As a result, the volume fraction of inclusions and the mean inclusion diameter on the fracture surface of the weldment are larger for weldments made with CO_2 shielding gas. Furthermore, reduction in the alloy content of the weldment because of oxidation leads to a less desirable microstructure. These effects have been quantified using a series of techniques presented in this report.

There still remains some question as to the relative importance of inclusions and microstructure in influencing toughness. Although the weldment fabricated in CO_2 had a larger volume fraction of inclusions than the one made in Ar-2%O_2, the mean linear intercept dimple size on the fracture surface was the same for both weldments. The microstructure of the weldment made in CO_2 was more massive than that of the weldment made with Ar-2%O_2. The variations in alloy content and microstructure between the two weldments resulted in a variation in the work hardening coefficient. The explanation for the toughness results favored by the authors is that there were equal numbers of microvoid nuclei in both

weldments, but that the energy dissipated in growing the microvoids was different due to the variations in microstructure and alloy content. There may be other equally valid explanations for the results, however.

Further work will look at the temperature dependence of the features on a fracture surface to determine if the cut-off diameter is sensitive to temperature and how the volume fraction and size distribution of inclusions on the fracture surfaces are affected by temperature. A clearer separation of the effects of microstructure and inclusions may result from these studies.

Acknowledgment

The authors gratefully acknowledge the technical assistance of and many helpful discussions with H. I. Kaplan. The help of F. P. Carberry in preparing the weld samples is appreciated. Thanks are also due to D. J. Amborski and H. F. Hillery for their contributions in the areas of optical and electron microscopy.

References

1. Lewis, W. J., Faulkner, G. E., Martin, D. C., and Rieppel, P. J., "Submerged Arc Welding HY-80 Steel," *Weld. Jour.* 39 (6), 1960, Res. Suppl., 266-s.

2. Sibley, C. R., "Welding HY-80 Steel with the Gas-Shielded Metal Arc Process," *Weld. Jour.* 42 (5), 1963, Res. Suppl., 219-s.

3. Nelson, J. W., Randall, M.D., and Martin, D. C., "Development of Methods of Making Narrow Welds in Thick Steel Plates by Automatic Arc Welding Processes," *Final Report to Bureau of Ships, Dept. of the Navy, Contract NObs-86424,* 1964, Battelle Memorial Institute.

4. Sagan, S. S. and Campbell, H. C., "Factors Which Affect Low-Alloy Weld-Metal Notch-Toughness," *Bulletin No. 59,* 1960, Welding Research Council.

5. Dorschu, K. E. and Stout, R. D., "Some Factors Affecting the Notch Toughness of Steel Weld Metal," *Weld. Jour.* 40 (3), 1961, Res. Suppl., 97-s.

6. Ohwa, T., "Statistical Investigation on the Effect of Alloying Elements for the Notch-Toughness of Weld Metal," *Document II-221-62,* 1962, Commission II of the Int. Inst. of Welding.

7. Garstone, J. and Johnson, F. A., "Impact Properties of Mild Steel Weld Metals," *Brit. Weld. Jour.* 10 (5), 1963, 224.

8. Kubli, R. A. and Sharar, W. B., "Advancements in Submerged-Arc Welding of High-Impact Steels," *Weld. Jour.* 40 (11), 1961, Res. Suppl., 497-s.

9. Heuschkel, J., "Weld Metal Property Selection and Control," *Weld. Jour.* 52 (1), 1973, Res. Suppl., 1-s.

10. Russ, J.C., "Comparison of Fractographic Techniques," *Microstructures,* 1971, 13.

11. Krafft, J. M., "Correlation of Plane-Strain Crack Toughness with Strain Hardening Characteristics of a Low, a Medium, and a High Strength Steel," *App. Mater. Res.* 3, 1964, 88.

12. Spitzig, W. A., "Correlations Between Fractographic Features and Plane-Strain Fracture Toughness in an Ultrahigh Strength Steel," *STP 453,* 1969, Amer. Soc. for Testing and Materials.

13. Birkle, A. J., Wei, R. P., and Pellissier, G. E., "Analysis of Plane-Strain Fracture in a Series of 0.45 C-Ni-Cr-Mo Steels with Different Sulfur Contents," *Trans. ASM* 59, 1966, 981.

14. Passoja, D. E. and Hill, D. C., "On the Distribution of Energy in the Ductile Fracture of High Strength Steels," submitted to *Met. Trans.*

15. Edelson, B. I., and Baldwin, W. M., "The Effect of Second Phases on the Mechanical Properties of Alloys," *Trans. ASM* 55, 1962, 230.

16. Gladman, T., Holmes, B., and McIvor, I. D., "Effects of Second Phase Particles on Strength, Toughness and Ductility," *Rept. No. 145,* 1971, Iron and Steel Institute.

17. Gray, J. M. and Wilson, W. G., "Evaluation of an X-80 Arctic Pipeline Steel Containing 0.10 Percent Columbium," *Petroleum Mechanical Engineering Conference,* 1973, ASME.

18. Widgery, D. J., "Deoxidation Practice and Toughness of Mild Steel Weld Metal," *Rept. No. M/76/73,* 1973, The Welding Institute.

19. Turkdogan, E. T., "Nucleation, growth and flotation of oxide inclusions in liquid steel," *JISI,* 1966, 914.